

# Tropospheric Refraction Modeling Using Ray-Tracing and Parabolic Equation

Pavel VALTR, Pavel PECHAČ

Dept. of Electromagnetic Field, Czech Technical University in Prague, Technická 2, 166 27 Praha 6, Czech Republic

valtrp@fel.cvut.cz, pechac@fel.cvut.cz

**Abstract.** *Refraction phenomena that occur in the lower atmosphere significantly influence the performance of wireless communication systems. This paper provides an overview of corresponding computational methods. Basic properties of the lower atmosphere are mentioned. Practical guidelines for radiowave propagation modeling in the lower atmosphere using ray-tracing and parabolic equation methods are given. In addition, a calculation of angle-of-arrival spectra is introduced for multipath propagation simulations.*

## Keywords

Radiowave propagation, Tropospheric refraction, Ray-tracing, Parabolic equation.

## 1. Introduction

Long-range electromagnetic wave propagation in near-horizon direction is largely governed by spatial distribution of the refractive index in the atmosphere. Consideration of refractive properties of the lower atmosphere is thus of certain importance when planning and designing terrestrial communication systems mainly because of multipath fading and interference effects due to trans-horizon propagation. Multipath phenomena can also be used for remote sensing applications.

Recent propagation modeling methods considering the refractive properties of the atmosphere employ ray-tracing and parabolic equation approach. Ray-tracing is a geometrical optics method while the parabolic equation method is a full-wave approach to a homogeneous wave equation solution. Both methods have been known for many years, but new applications place new requirements on their implementation: multipath phenomena precise modeling, horizontally inhomogeneous troposphere, etc.

This paper provides a basic description of methods used in radiowave propagation prediction, taking into account the refractive conditions of atmosphere. Ray-tracing and parabolic equation methods as the most widely used techniques are addressed including implementation issues. Practical guidelines are given to enable the selection of a

proper method and its implementation for a specific application. At the end a method for angle-of-arrival spectra calculation is presented for precise multipath propagation simulations.

## 2. Radio Refractive Index

The troposphere forms the lowest part of the atmosphere from the surface of the earth up to several km. From the propagation point of view, the troposphere is characterized by a refractive index, whereas the rate of the change of the refractive index with height is of crucial importance. The refractive index itself depends on absolute temperature, atmospheric pressure and partial pressure due to water vapor [1]. The predominant dependence of these quantities on elevation makes the troposphere a mostly horizontally stratified media. The refractive properties of air can be expressed in terms of the refractive index  $n$  or refractivity  $N$ , where

$$N = (n - 1) \cdot 10^6. \quad (1)$$

The refractive index of air at the surface of the earth is approximately 1.0003. Standard atmosphere is represented by an approximately linear decrease of refractivity at low altitudes with a long-term mean value of the refractivity gradient equal to  $-40$  N/km, [2], [3]. Radiowaves are bent in consequence of a non-constant refractive index. The effect of the refractivity gradient to wave bending can be expressed using the radius of curvature of a ray representing the electromagnetic wave. The radius of curvature  $\rho$  of the ray can be well approximated by [4]

$$\rho = -\frac{1}{dn/dz}. \quad (2)$$

The radius of the earth curvature is  $\rho_e = 6378$  km. The radius of the curvature of the ray under standard gradient is higher than the radius of the earth curvature; both radii are equal for  $dN/dz = -157$  N/km. The definition of modified refractivity and modified refractive index comes from

$$M = N + 157z, \quad M = (m - 1) \cdot 10^6 \quad (3)$$

where  $M$  and  $m$  are modified refractivity and modified refractive index, respectively, and  $z$  is height in km.

The effects of various refractivity gradients can be seen in Fig. 1, where bending of rays representing radio waves is shown relative to earth curvature. The rays propagating under positive refractivity gradients are bent upwards. The standard refractivity gradient causes rays to bend downwards, but the curvature of the earth ( $1/\rho_e$ ) exceeds the curvature of the ray ( $1/\rho$ ), which prevents trans-horizon propagation and creates a shadow area behind the radio horizon range. Ray propagating under a refractivity gradient equal to  $dN/dz = -157$  N/km is exactly parallel to the surface of the earth. Gradients of less than  $-157$  N/km produce ducting where the curvature of the rays exceeds the curvature of the earth and the wave travels for a very long distance behind the radio horizon.

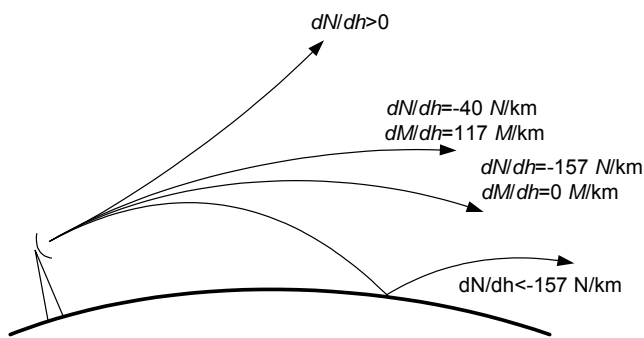


Fig. 1. Rays under various refractivity gradients.

Basically, there are two effects that can break the standard situation of the constant gradient of refractivity. The first is an abrupt decrease of water vapor pressure with height, which occurs mostly in a narrow layer over water surface and results in a so called evaporation duct, Fig. 2(a). The other is an inverse increase of temperature with height causing a surface or elevated duct, Fig. 2(b,c). Range of heights of the ducting layer is determined by the top of negative  $M$  gradient layer and height of equal  $M$  below [5].

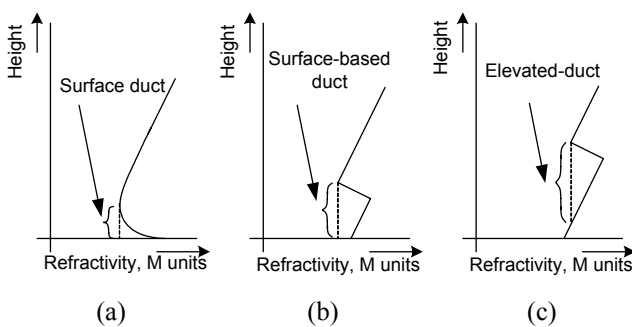


Fig. 2. Types of ducts.

### 3. Geometrical Optics

Geometrical optics is a method suitable for the treatment of propagation problems in homogenous media or in slowly varying media compared to wavelength. The propagating field is locally considered a plane wave represented by rays. Rays form trajectories perpendicular to the wave

front at each point. Considering a high frequency harmonic field in inhomogeneous media and assuming small variations of field intensity amplitude compared to wavelength (large wavenumber  $k_0$ ) leads to the following pair of equations determining the ray trajectory in two dimensions [6]

$$\frac{d}{ds} \left( n(z) \frac{dx}{ds} \right) = \frac{\partial n(z)}{\partial x}, \quad \frac{d}{ds} \left( n(z) \frac{dz}{ds} \right) = \frac{\partial n(z)}{\partial z} \quad (4)$$

where only the dependence of refractive index on height  $z$  is considered and where  $s$  represents the length of the arc of the ray and  $x$  denotes the horizontal distance. The left term of the first equation equals to zero causing the bracketed term to be constant

$$n(z) \frac{dx}{ds} = n(z) \cos \theta = C \quad (5)$$

where  $C$  is a constant and  $\theta$  is the angle of the ray from horizontal direction. Eq.(5) represents Snell's law. Considering the piece-wise linear profile in Fig. 3(a), the dependence of the refractive index in the horizontal segment is in the form

$$n_2 = n_1 + \delta(z_2 - z_1) \quad (6a)$$

where  $\delta$  is the refractive index gradient. Inserting (6a) into Snell's law, the following set of equations determining the trajectory of the ray in one of the linear segments can be derived [7]

$$x_2 = x_1 + (\alpha_2 - \alpha_1) / \delta \quad (6b)$$

$$\alpha_2^2 = \alpha_1^2 + 2(n_2 - n_1) \quad (6c)$$

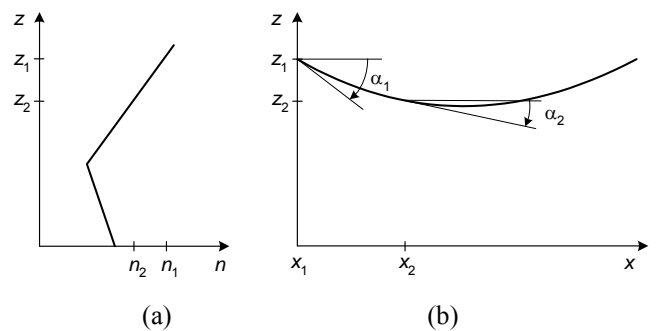


Fig. 3. Refractive index profile and bending of a ray

Eq. (6b) represents the dependence of  $x$  on the respective angle  $\alpha_2$ , which is in turn determined by the initial angle  $\alpha_1$  (6c). If the turn-around point of the ray exists within one layer as in Fig. 3(b), the two particular paths of the ray have to be treated separately. Possible ground reflections of the ray have to be considered.

In the formulas above, a rectangular coordinate system rather than a spherical one was considered. To be able to work with the flat earth model, the refractive index  $n$  has to be replaced by a modified refractive index  $m$  [7]. Fig. 4 shows the case of a standard atmosphere. Ray paths obtained using (6a-c) are shown with the rays bent upwards under earth flattening transformation. Fig. 5 shows an

example of a refractivity profile with the ducting layer extending from 50 to 70 m. The tropospheric waveguide effect causing the wave to travel far beyond the horizon can be seen.

Although ray-tracing provides a rather simple tool for finding the path of individual rays, problems may arise when treating diffraction effects caused by terrain irregularity and earth curvature. In such a case the principles of diffraction theory must be employed. Furthermore, a single ray carries no amplitude information, and amplitude is derived from the cross section of a tube of rays formed by several rays. In addition, geometrical optics does not provide correct results at a ray caustic, i.e. at a locus of zero cross-section of the ray tube.

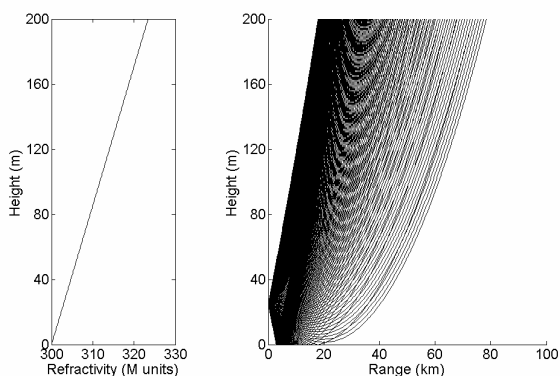


Fig. 4. Ray paths under a standard refractivity profile.

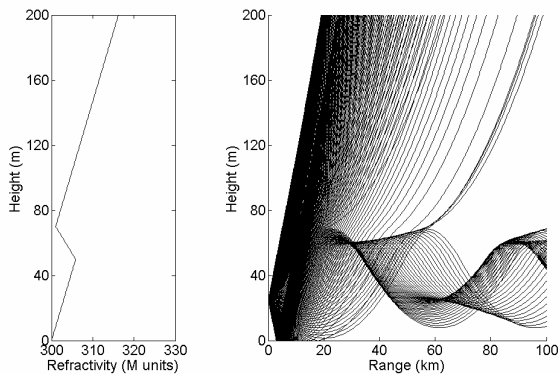


Fig. 5. Ray paths in presence of ducting layer.

In the next section, a description of an alternative approach to the solution of radiowave propagation modeling based on the full-wave solution of a reduced wave equation is presented.

## 4. Parabolic Equation

Because of the large computation domains involved in radiowave propagation modeling in the troposphere, it is usually impossible to solve Maxwell's equations or wave equation directly. Alternative approaches must be utilized to obtain the solution in reasonable time. Considering the

received power prediction in a terrestrial point-to-point radio link, radar-cross-section computation and other related propagation problems, the area of interest is within several degrees of the preferred direction. In such a case a reduced wave equation of the parabolic type can be handled to obtain a computationally effective solution.

A two-dimensional scalar wave equation in the Cartesian coordinate system can be written as

$$\frac{\partial^2 \psi}{\partial x^2} + \frac{\partial^2 \psi}{\partial z^2} + k_0^2 n^2 \psi = 0 \quad (7)$$

where  $\psi$  is the electric or magnetic field component,  $k_0$  is the wavenumber in a vacuum,  $n$  is the refractive index,  $x$  and  $z$  denote the axes representing distance and height, respectively. Considering the solution to (7) in the form of

$$\psi(x, z) = u(x, z) \cdot e^{-jk_0 x} \quad (8)$$

where  $x$  represents the predominant direction of propagation and inserting it to (7) the results is

$$\frac{\partial^2 u}{\partial x^2} - 2jk_0 \frac{\partial u}{\partial x} + \frac{\partial^2 u}{\partial z^2} + k_0^2 (n^2 - 1) u = 0 \quad (9)$$

Eq. (9) can be formally written as

$$\left[ \frac{\partial}{\partial x} - jk_0(1-Q) \right] \left[ \frac{\partial}{\partial x} - jk_0(1+Q) \right] u = 0 \quad (10)$$

representing a forward and backward traveling wave, where  $Q = \sqrt{(1/k_0^2) \partial^2 / \partial z^2 + n^2}$ . Considering only the forward traveling wave, we obtain

$$\frac{\partial u}{\partial x} = jk_0 (1 - \sqrt{1+Q'}) u \quad (11)$$

where  $Q' = (1/k_0^2) \partial^2 / \partial z^2 + n^2 - 1$ . Inserting the two-terms Taylor approximation

$$\sqrt{1+Q'} \approx 1 + Q'/2 \quad (12)$$

in (11) provides the parabolic equation

$$\frac{\partial^2 u}{\partial z^2} - 2jk_0 \frac{\partial u}{\partial x} + k_0^2 (n^2 - 1) u = 0 \quad (13)$$

The parabolic equation approach to solve propagation problems is suitable for cases of long-range propagation under narrow propagation angles. Compared to the ray-tracing technique it provides an efficient tool for solving problems including both terrain diffraction and refraction phenomena. The two implementations that are used to numerically solve (13) based on finite differences and Fourier transform are briefly described in the next sections.

### 4.1 Finite-Difference Implementation

Eq. (13) is solved numerically by the Crank-Nicolson schema using a rectangular grid, Fig. 6. The differentiations in (13) are expressed as:

$$\frac{\partial u_{i+1/2}^m}{\partial x} = \frac{u_{i+1}^m - u_i^m}{\Delta x} \quad (14a)$$

$$\frac{\partial^2 u_{i+1/2}^m}{\partial z^2} = \frac{u_i^{m-1} - 2u_i^m + u_i^{m+1} + u_{i+1}^{m-1} - 2u_{i+1}^m + u_{i+1}^{m+1}}{2\Delta z^2} \quad (14b)$$

$$u_{i+1/2}^m = \frac{u_i^m + u_{i+1}^m}{2}. \quad (14c)$$

The computation is performed by steps: a field on a vertical in the next step, denoted by  $i+1$  subscript is computed from the field in the previous step  $i$  with given boundary conditions at the bottom and top of the computational domain and with given field distribution at the initial vertical plane.

Inserting the above equations in (13) and rearranging the  $i$  and  $i+1$  terms gives

$$\begin{aligned} u_{i+1}^{m-1} + (-2 - a + b_i^m)u_{i+1}^m + u_{i+1}^{m+1} &= \\ = -u_i^{m-1} + (2 - a - b_i^m)u_i^m - u_i^{m+1} \end{aligned} \quad (15)$$

where

$$a = 4jk_0\Delta z^2/\Delta x \quad (16a)$$

$$b_i^m = k_0^2(n_{i+1/2}^m - 1)\Delta z^2. \quad (16b)$$

$\Delta x$  and  $\Delta z$  are step sizes in horizontal and vertical directions respectively,  $n$  represents the vector of refractive index height dependence at a given range. Eq. (15) can be written in matrix form as

$$[A_i] \cdot [u_{i+1}] = [B_i] \cdot [u_i] \quad (17)$$

where

$$A_i = \begin{bmatrix} \alpha_i^1 & 1 & 0 & 0 & \dots & 0 & 0 & 0 & 0 \\ 1 & \alpha_i^2 & 1 & 0 & \dots & 0 & 0 & 0 & 0 \\ 0 & 1 & \alpha_i^3 & 1 & \dots & & & & 0 \\ \dots & & & & & & & & \dots \\ 0 & 0 & & & \dots & 1 & \alpha_i^{N-2} & 1 & 0 \\ 0 & 0 & 0 & & \dots & 0 & 1 & \alpha_i^{N-1} & 1 \\ 0 & 0 & 0 & 0 & \dots & 0 & 0 & 1 & \alpha_i^N \end{bmatrix} \quad (18a)$$

and

$$B_i = \begin{bmatrix} \beta_i^1 & 1 & 0 & 0 & \dots & 0 & 0 & 0 & 0 \\ 1 & \beta_i^2 & 1 & 0 & \dots & 0 & 0 & 0 & 0 \\ 0 & 1 & \beta_i^3 & 1 & \dots & & & & 0 \\ \dots & & & & & & & & \dots \\ 0 & 0 & & & \dots & 1 & \beta_i^{N-2} & 1 & 0 \\ 0 & 0 & 0 & & \dots & 0 & 1 & \beta_i^{N-1} & 1 \\ 0 & 0 & 0 & 0 & \dots & 0 & 0 & 1 & \beta_i^N \end{bmatrix} \quad (18b)$$

where

$$\alpha_i^m = -2 - a + b_i^m \quad (19a)$$

$$\beta_i^m = 2 - a - b_i^m. \quad (19b)$$

The resulting field in the next step  $u_{i+1}$  is obtained by matrix inversion of (17). Because of the rectangular grid modified refractive index  $m$  must be used instead of the refractive index  $n$  to account for the earth curvature.

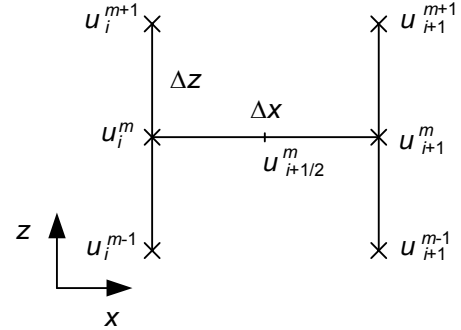


Fig. 6. Discretisation finite-difference grid.

## 4.2 Fourier Transform Implementation

Defining Fourier transform of the function  $u(x, z)$  as

$$U(x, p) = \mathcal{F}\{u(x, z)\} = \int_{-\infty}^{\infty} u(x, z) e^{-j p z} dz \quad (20)$$

and making use of the identities

$$\mathcal{F}\{\partial^2 u / \partial z^2\} = -p^2 U \quad (21a)$$

$$\mathcal{F}\{\partial u / \partial x\} = (\partial / \partial x) U \quad (21b)$$

eq. (13) can be Fourier-transformed as

$$-p^2 U(x, p) - 2jk_0 \frac{\partial U(x, p)}{\partial x} + k_0^2 (n^2 - 1) U(x, p) = 0 \quad (22)$$

The solution to this differential equation can be obtained in closed form

$$U(x, p) = e^{j p^2 x / 2 k_0} \cdot e^{-j k_0 (n^2 - 1) x / 2}. \quad (23)$$

The field on the vertical in the next step is then obtained from field values in the previous step as

$$u(x + \Delta x, z) = e^{-j k_0 (n^2 - 1) \Delta x / 2} \cdot \mathcal{F}^{-1} \left\{ e^{j p^2 \Delta x / 2 k_0} \cdot \mathcal{F}\{u(x, z)\} \right\} \quad (24)$$

and the computation is marched in horizontal direction in the same way as in the case of finite-differences. Fourier transform of a plane wave of unit amplitude propagating in a vacuum at angle  $\theta$  is

$$\mathcal{F}\{e^{j k_0 x \cos \theta} \cdot e^{j k_0 z \sin \theta}\} = e^{j k_0 x \cos \theta} \delta(p - k_0 \sin \theta) \quad (25)$$

where  $\delta$  is a Dirac function. The variable  $p = k_0 \sin(\theta)$  has the meaning of an angle frequency corresponding to a wave traveling at the angle  $\theta$ . When employing Fast Fourier Transform for marching (24), the maximum angle of propagation  $\theta_{\max}$  must be chosen. The vertical spacing of the computation grid  $\Delta z$  must be chosen accordingly

$$\Delta z \leq \pi/p_{\max} = \pi/(k_0 \sin \theta_{\max}). \quad (26)$$

Radiation pattern of transmitting antenna can be incorporated into the parabolic equation model by setting an appropriate field distribution of the initial vertical plane. Supposing the radiation pattern is  $P(p)$  where  $p = k_0 \sin(\theta)$  and  $\theta$  is an angle, the initial field is

$$f(z) = F^{-1}\{P(p - p_e)\} \quad (27)$$

where  $p_e$  is the angle frequency corresponding to the elevation angle of the antenna  $\theta_e$ ,  $f(z)$  is the field distribution of the initial vertical corresponding to zero height of the transmitter. The field distribution corresponding to antenna at height  $z_h$  is obtained by the appropriate shifting of  $f(z)$

$$u(0, z) = f(z - z_h). \quad (28)$$

Parabolic equation results in form of relative received power (dB) were obtained using Fourier transform implementation considering horizontal polarization, frequency 10 GHz and perfectly conducting ground. The horizontal step was 200 m. Fig. 7. shows the situation of a standard atmosphere corresponding to the ray-tracing result in Fig. 4. An identical depiction with earth curvature shown is in Fig. 8.

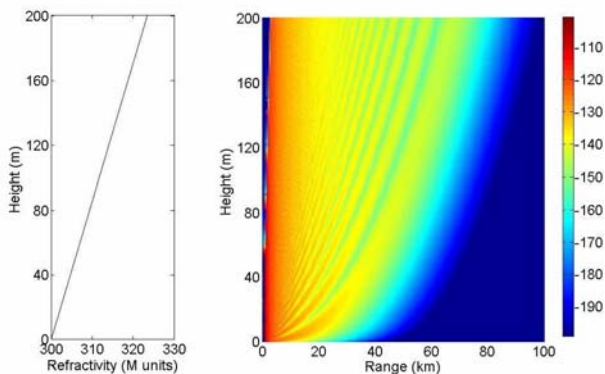


Fig. 7. Relative received power (dB), flat earth.

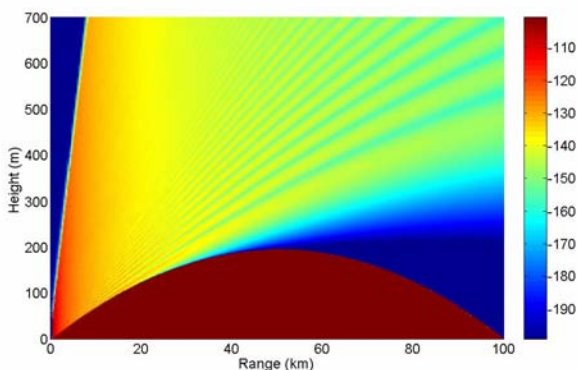


Fig. 8. Relative received power (dB), earth's curvature depicted.

### 4.3 Implementation Issues

In the tropospheric propagation modeling the need for numerical efficient algorithms is of crucial importance. Fourier transform based algorithms allow larger range steps than the finite-difference methods and they are computationally more effective. The range step for finite-differences is 10-100 wavelengths. A Fourier transform implementation range step can be up to 900 m and 270 m for lower and higher frequencies, respectively [8]. Terrain profile can be easily incorporated in the following way: the field on the vertical in the next step is computed considering no presence of the terrain. Grid points at the bottom of the discretisation grid corresponding to the terrain height at the given range are then set to zero. This approach allows only staircase approximation of the terrain. More precise terrain modeling is also possible [7]. Matrices (16) are valid for a perfectly conducting flat earth surface. Reflections from the surface represented by permittivity and conductivity at a lower boundary can be implemented by direct inserting of a Leontovich boundary condition into the first line in of matrix  $A$  and  $B$  in (16). A mixed Fourier transform [9], [10] is used to model impedance boundary when using Fourier transform implementation. To prevent reflections from the upper boundary the field must be gradually attenuated towards the top of the grid. Usually a Hanning window is used to create the attenuation layer.

Although the Fourier transform approach can not be used in the general case of more complicated boundaries, where finite-difference method must be used, this usually causes no problems in long-range propagation modeling where usually only the air-earth boundary is considered.

## 5. Angle-of-Arrival

One of the factors limiting the performance of line-of-sight communication systems is multipath propagation occurrence. The multipath is derived from two basic mechanisms, namely ground reflection and atmospheric refraction. One way to detect a multipath is by angle-of-arrival measurement. The angle-of-arrival spectrum has a meaning of directions from which the wave arrives at the receiving point of the link. It represents an angular spectrum of plane waves hitting the aperture of the receiving antenna. The concept of the angle-of-arrival measurement is described in [11]. From ray-tracing the angles of rays are obtained directly by the means described in Sec. 3. When performing a parabolic equation simulation, the angle-of-arrival spectrum is computed by the method described below.

Consider two plane waves carrying amplitudes  $a_1$  and  $a_2$  arriving at a vertical antenna array as shown in Fig. 9 with the geometry shown in Fig. 10.

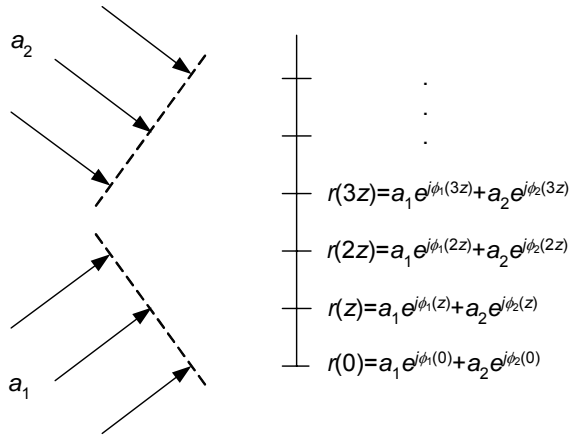


Fig. 9. Two plane waves arriving at an antenna array.

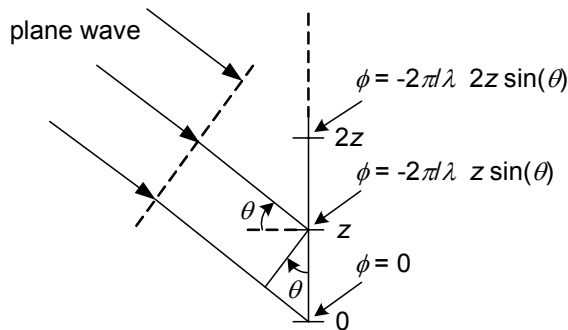


Fig. 10. Plane wave geometry.

Setting the phase  $\Phi$  at the lowest element of the antenna array to zero, the received field at the individual elements can be expressed as

$$\begin{aligned}
 r(0) &= a_1 + a_2 \\
 r(z) &= a_1 e^{jk_0 z \sin(\theta_1)} + a_2 e^{-jk_0 z \sin(\theta_2)} \\
 r(2z) &= a_1 e^{jk_0 2z \sin(\theta_1)} + a_2 e^{-jk_0 2z \sin(\theta_2)} \\
 r(3z) &= a_1 e^{jk_0 3z \sin(\theta_1)} + a_2 e^{-jk_0 3z \sin(\theta_2)}
 \end{aligned}
 \tag{29}$$

The spacing between the elements of the array is  $z$ ,  $\theta_1$  and  $\theta_2$  are the respective angles of incidence of the plane waves. Vector  $r$  forms the sampled sum of harmonic functions. The Fourier transform of this vector represents an angular spectrum of incident plane waves with spectral lines at angles  $\theta_1$  and  $\theta_2$ . To fulfill the sampling theorem the spacing must be

$$z \leq \lambda / (2 \sin \theta_{\max})
 \tag{30}$$

where  $\theta_{\max}$  is the maximum angle of incidence which is usually bounded below one degree in the long-range tropospheric propagation case.

To demonstrate the relation between fading and multipath, see the height dependence of the relative received power (dB) at a distance of 30 km from the 10 GHz transmitter at a height of 25 m for a standard atmosphere in Fig.11 obtained using the parabolic equation.

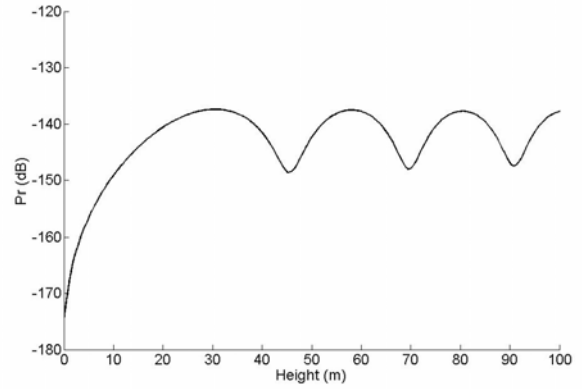


Fig. 11. Height dependence of relative received power.

The minima in Fig. 11 are caused by phase summation of the direct and ground-reflected wave. Corresponding normalized angle-of-arrival spectra computed from the simulated values and using a Dolph-Tschebyscheff filter to reduce sidelobes are shown in Fig. 12.

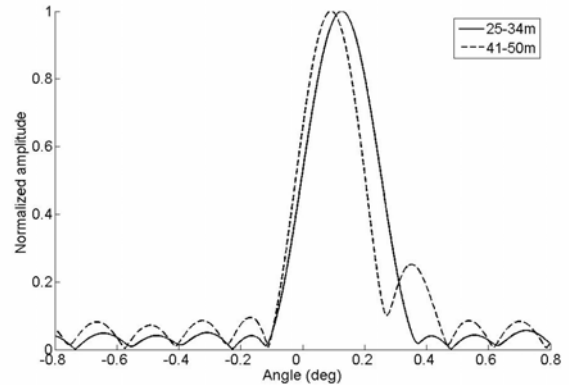


Fig. 12. Angle-of-arrival spectra.

The solid and dotted lines represent angle-of-arrival spectra corresponding to a 10-element vertical antenna array aperture extending from 25 m to 34 m and from 41 m to 50 m, respectively. It can be seen that two peaks corresponding to direct and ground reflected wave exist in the latter case, giving rise to the minimum of the received power in the respective range of heights, see Fig. 11.

## 6. Conclusion

Prospective wireless communication systems require precise radiowave propagation modeling in the troposphere. The advancement of computers allows new approaches to the implementation of classical modeling methods to satisfy new demands on precise propagation prediction. This paper provided the corresponding basic computational tools and guidelines. The method of computation of angle-of-arrival spectra from simulation results obtained by parabolic equation method was introduced. As an example, the multipath phenomena modeling can be used for remote sensing of the refractivity height profiles in

the troposphere [12]. Recently, great attention has also been given to refractivity profile measurement, so new requirements for radiowave propagating modeling in the troposphere can be expected in the near future.

## Acknowledgements

This work has been partially supported by the Czech Ministry of Education, Youth and Sports in the frame of the project MSM 6840770014 "Research in the Area of the Prospective Information and Navigation Technologies" (ray tracing modeling) and by the Czech Science Foundation grant No. 102/04/2153 "Time-space Simulations of MWS Systems in 42 GHz Band" (parabolic equation modeling).

## References

- [1] KERR, D. E. *Propagation of Short Radio Waves*. New York: McGraw-Hill, 1951.
- [2] GRABNER, M., KVICERA, V. Refractive index measurement at the Prague TV tower. *Radioengineering*. 2003, vol. 12, no. 1, pp. 5-7.
- [3] REZACOVA, D., FISER, O., RAMON SAEZ, L. Statistics of radio refractivity derived from Prague radiosounding data. *Radioengineering*. 2003, vol. 12, no. 4, pp. 84-88.
- [4] LIVINGSTON, D. C. *The Physics of Microwave Propagation*. New Jersey: Prentice-Hall, 1970.
- [5] HITNEY, H. V., RICHTER, J. H., PAPPERT, R. A., ANDERSON, K. D., BAUMGARTNER, G. B. Tropospheric radio propagation assessment. *Proc. IEEE*. 1985, vol. 73, no. 2, pp. 265-283.
- [6] JONES, D. S. *Methods in Electromagnetic Wave Propagation*. 2<sup>nd</sup> ed. Wiley-IEEE Press, 1994.
- [7] LEVY, M. F. *Parabolic Equation Methods for Electromagnetic Wave Propagation*. London: IEE Press, 2000.
- [8] BARRIOS, A. E. Parabolic Equation modelling in horizontally inhomogeneous environments. *IEEE Transactions on Antennas and Propagation*. 1992, vol. 40, no. 7, pp. 791-797.
- [9] KUTTLER, J. R., DOCKERY, G. D. Theoretical description of the parabolic approximation/Fourier split-step method of representing electromagnetic propagation in the troposphere. *Radio Science*. 1991, vol. 26, no. 2, pp. 381-393.
- [10] DOCKERY, G. D., KUTTLER, J. R. An improved impedance-boundary algorithm for Fourier split-step solutions of the parabolic wave equation. *IEEE Transactions on Antennas and Propagation*. 1996, vol. 44, no. 12, pp. 1592-1599.
- [11] WEBSTER, A. R. Angles-of-arrival and tropospheric multipath microwave propagation. *IEEE Transactions on Antennas and Propagation*. 1987, vol. 35, no. 1, pp. 94-99.
- [12] VALTR, P., PECHAČ, P. Novel method of vertical refractivity profile estimation using angle of arrival spectra. In *XXVIIIth General Assembly of International Union of Radio Science [CD-ROM]*. New Delhi (India), 2005.

## About Authors...

**Pavel VALTR** received his M.Sc. degree from the Czech Technical University in Prague in 2004. Now he is working towards his Ph.D. at the Department of Electromagnetic Field of the same university. His main interest is in radiowave propagation modeling.

**Pavel PECHAČ** graduated at the Czech Technical University in Prague in 1993. He received his Ph.D. in Radio electronics in 1999 at the Department of Electromagnetic Field. He is with the department as an associate professor. His research interests have been in the field of radiowave propagation and wireless systems.